NASA/TM–20250008926

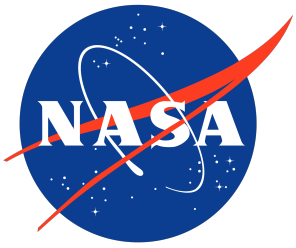

# Using Doppler Tracking to Aid Trajectory Reconstruction for Atmospheric Entry, Descent, and Landing

*Elan M. Graupe*
*University of Minnesota, Minneapolis, Minnesota*

*Christopher D. Karlgaard*
*Analytical Mechanics Associates, Hampton, Virginia*

*Soumyo Dutta*
*NASA Langley Research Center, Hampton, Virginia*

September 2025

**NASA STI Program Report Series**

Since its founding, NASA has been dedicated to the advancement of aeronautics and space science. The NASA scientific and technical information (STI) program plays a key part in helping NASA maintain this important role.

The NASA STI Program operates under the auspices of the Agency Chief Information Officer. It collects, organizes, provides for archiving, and disseminates NASA's STI. The NASA STI Program provides access to the NTRS Registered and its public interface, the NASA Technical Report Server, thus providing one of the largest collections of aeronautical and space science STI in the world. Results are published in both non-NASA channels and by NASA in the NASA STI Report Series, which includes the following report types:

- TECHNICAL PUBLICATION. Reports of completed research or a major significant phase of research that present the results of NASA programs and include extensive data or theoretical analysis. Includes compilations of significant scientific and technical data and information deemed to be of continuing reference value. NASA counterpart of peer-reviewed formal professional papers, but having less stringent limitations on manuscript length and extent of graphic presentations.
- TECHNICAL MEMORANDUM. Scientific and technical findings that are preliminary or of specialized interest, e.g., quick release reports, working papers, and bibliographies that contain minimal annotation. Does not contain extensive analysis.
- CONTRACTOR REPORT. Scientific and technical findings by NASA-sponsored contractors and grantees.
- CONFERENCE PUBLICATION. Collected papers from scientific and technical conferences, symposia, seminars, or other meetings sponsored or co-sponsored by NASA.
- SPECIAL PUBLICATION. Scientific, technical, or historical information from NASA programs, projects, and missions, often concerned with subjects having substantial public interest.
- TECHNICAL TRANSLATION. English-language translations of foreign scientific and technical material pertinent to NASA's mission.

Specialized services also include organizing and publishing research results, distributing specialized research announcements and feeds, providing information desk and personal search support, and enabling data exchange services.

For more information about the NASA STI Program, see the following:

- Access the NASA STI program home page at `http://www.sti.nasa.gov`
- Help desk contact information: `https://www.sti.nasa.gov/sti-contact-form/` and select the "General" help request type.

NASA/TM–20250008926

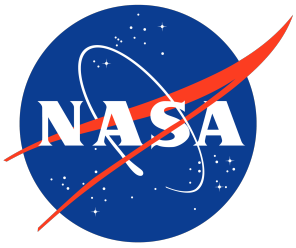

# Using Doppler Tracking to Aid Trajectory Reconstruction for Atmospheric Entry, Descent, and Landing

*Elan M. Graupe*
*University of Minnesota, Minneapolis, Minnesota*

*Christopher D. Karlgaard*
*Analytical Mechanics Associates, Hampton, Virginia*

*Soumyo Dutta*
*NASA Langley Research Center, Hampton, Virginia*

National Aeronautics and
Space Administration

Langley Research Center
Hampton, Virginia 23681-2199

September 2025

## Acknowledgments

The authors are grateful to Entry Systems Modeling project for funding part of the work in this paper. The authors also would like to thank Ronald Neale of NASA Langley Research Center for assistance in creating the graphics in Figure 2.



Available from:

NASA STI Program / Mail Stop 150
NASA Langley Research Center
Hampton, VA 23681-2199

## Abstract

A Doppler tracking measurement model is presented for an Iterative Extended Kalman Filter or an Iterative Unscented Kalman Filter. Doppler tracking refers to the tracking of the Doppler shift in a spacecraft's radio communications as they travel from the transmitting antenna to the receiving antenna. Radio signals experience a deterministic Doppler shift when there is a non-zero relative velocity between the transmitting antenna and receiving antenna. Measurements of the Doppler shift at a receiving antenna on Earth can therefore be used to estimate modes of the velocity of the spacecraft broadcasting those signals. The measurement model presented in this work enables the use of Doppler shift measurements in the trajectory reconstruction of an atmospheric entry vehicle. The Doppler tracking measurement model is implemented in the New Statistical Trajectory Estimation Program, which is a trajectory reconstruction software developed at NASA Langley Research Center. The measurement model's efficacy is evaluated using simulated data from a six degree-of-freedom vehicle model of the Huygens probe as well as the actual Doppler data collected by the Huygens Doppler Winds Experiment.

# Contents

# List of Tables



# List of Figures

## Nomenclature

| | | |
|---|---|---|
| $(\bullet)^T$ | = | The transpose of matrix $(\bullet)$ |
| $(\bullet)_k$ | = | The value of $(\bullet)$ at the $k^{th}$ time step |
| $\dot{(\bullet)}$ | = | The first time derivative of $(\bullet)$ |
| $\mathbf{x}$ | = | Bold font indicates a matrix or vector quantity |
| $\mathbf{T}_a^b$ | = | Transformation matrix from frame $a$ to frame $b$ |
| $\mathbf{0}_{a,b}$ | = | Matrix of zeros with dimensions $a$ x $b$ |
| $< \mathbf{a}, \mathbf{b} >$ | = | The inner product of vectors $\mathbf{a}$ and $\mathbf{b}$ |
| $\|\|(\bullet)\|\|_2$ | = | The 2-norm of $(\bullet)$ |

## Abbreviations

| | | |
|---|---|---|
| API | = | Application Programming Interface |
| DTWG | = | Descent Trajectory Working Group |
| ECEF | = | Earth-centered Earth-fixed |
| EDL | = | Entry, Descent, and Landing |
| GPS | = | Global Positioning System |
| IAU | = | International Astronomical Union |
| IEKF | = | Iterative Extended Kalman Filter |
| IMU | = | Inertial Measurement Unit |
| INS | = | Inertial Navigation System |
| ITRF | = | International Terrestrial Reference Frame |
| IUKF | = | Iterative Unscented Kalman Filter |
| JPL | = | Jet Propulsion Laboratory |
| MICE | = | Matlab SPICE programming interface |
| NAIF | = | Navigation and Ancillary Information Facility |
| NED | = | North-East-Down |
| NewSTEP | = | New Statistical Trajectory Estimation Program |
| PCPF | = | Planet-Centered Planet-Fixed |
| PDS | = | Planetary Data System |
| POST2 | = | Program to Optimize Simulated Trajectories II |
| SPICE | = | Spacecraft, Planet, Instrument, C-Matrix, Events |

# 1 Introduction

After an entry, descent, and landing (EDL) sequence on a planetary body, a trajectory reconstruction is preformed to evaluate the performance of the entry vehicle. This reconstruction is typically done using an inertial measurement unit (IMU) consisting of an accelerometer triad and an gyroscope triad. These sensor measurements are fused using an inertial navigation system (INS). In these systems, the kinematic states of the vehicle (e.g., the position, velocity, and attitude) are tracked using a kinematics model that integrates the IMU measurements to determine how the states evolve over time. The accelerometer triad and gyroscope triad that make up the IMU contain errors in the form of stochastic noise and deterministic biases, which cause the inertial navigation solution to deviate significantly over extended periods of time. For this reason, additional sensors are used by the state estimation architecture to correct this drift. On Earth, a Global Positioning System (GPS), air data sensors, radar range and range-rate measurements are among the sensors available to perform this correction; however, the specific sensors used are highly dependent on the needs and limitations of the platform in question.

For entry systems entering Earth's atmosphere, measurements from a GPS receiver are paramount in this trajectory reconstruction because GPS receivers provide measurements that are directly related to the position and velocity of the Earth-entry vehicle [1]. These measurements can correct for drift and error accumulation in an INS. GPS measurements fused with the INS in a Kalman filtering framework are known as an INS/GPS fusion filter [2].

However, no such GPS constellation is available for entry systems traveling near other planetary bodies, like Mars, Venus or Titan. One potential solution is to use Doppler tracking to aid in the trajectory reconstruction. During the EDL maneuver, the entry vehicle usually sends telemetry to relay orbiters or receivers on Earth using radio communication. These radio waves experience a Doppler shift due to the relative velocity of the vehicle and the receiving antenna [3]. Various phases of the vehicle's trajectory can be extracted from this Doppler shift and used to aid in estimating the velocity and correcting for drift in the integration of the vehicle's inertial measurement unit data.

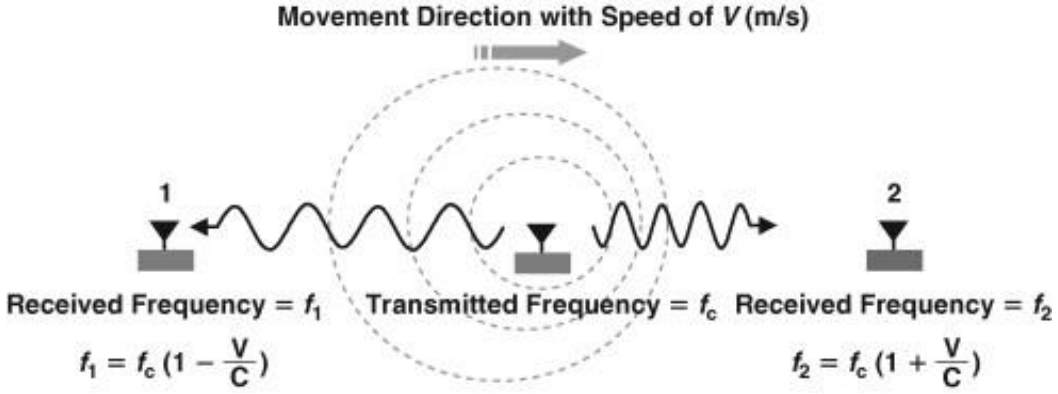


**Figure 1: Illustration of Doppler shift (figure reproduced from [4]).**

The concept of the Doppler shift measurement is illustrated in Figure 1. Here, a vehicle in motion emits a radio signal at a given frequency that is detected by two receivers. The motion of the vehicle compresses the radio waves in the direction of travel, resulting in a correspondingly higher frequency. Likewise the emitted waves opposite the vehicle motion are stretched, resulting in a lower frequency. Information about the vehicle's velocity can be inferred from the known emitted frequency and measurements of the frequency at the receiver location. Higher frequencies indicate motion toward the receiver and conversely a lower frequency indicates motion away from the receiver.

In this work, we describe a contribution to the New Statistical Trajectory Estimation Program (NewSTEP) [5–8] that adds the capability to utilize Doppler shift measurements in a trajectory reconstruction. NewSTEP, a trajectory reconstruction software developed at NASA Langley Research Center, is used to estimate the kinematic and atmospheric states of a vehicle during atmospheric entry, descent, and landing. At its core, NewSTEP is an INS/sensor fusion filter and smoother that is designed to reconstruct the trajectory a vehicle. Currently supported measurements include GPS, radar, temperature measurements, pressure measurements, magnetometer measurements, and flush air data systems.

The contribution described in this work is a Doppler tracking measurement model for the NewSTEP state estimation architecture. The Doppler tracking measurement model relates the measured Doppler shift of the radio transmission to the position and velocity of a vehicle. This model can be used in the measurement update of a filter to help correct for any inertial navigation errors.

The remainder of this report is organized as follows. In Section 2, we review the filter used in NewSTEP, including process models and the associated state vectors. In Section 3, we describe the Doppler tracking measurement model. Then, in Section 4, we describe a series of case studies. In the first case study, we implement Doppler tracking for a simulation of the Huygens probe during entry, descent, and landing. In the second case study, we use the Doppler tracking model on Doppler data collected by the Huygens Doppler Wind Experiment during Huygens's descent phase in January of 2005. Finally, in Section 5, we draw conclusions and suggest future work.

## 2 The NewSTEP Process Model

The NewSTEP trajectory reconstruction software supports either an Iterative Extended Kalman Filter (IEKF) or an Iterative Unscented Kalman Filter (IUKF). The details of the IEKF can be found in [5], and details on the implementation of the IUKF in NewSTEP can be found in [8]. Both the NewSTEP IEKF and the NewSTEP IUKF utilize the same set of system dynamics equations to govern the evolution of the vehicle state. The state dynamics are defined by a state vector $\mathbf{x}$, an input vector, and a set of differential equations to describe the evolution of the state vector.

The NewSTEP state vector $\mathbf{x}$ includes the inertial velocity of the vehicle $(u, v, w)$, the position $(r, \phi, \theta)$ of the vehicle, the attitude $(\mathbf{q})$ of the vehicle, the atmospheric

wind vector ($\mathbf{w}_{ned}$), the static atmospheric pressure ($p_\infty$), and the freestream density ($d_\infty$) of the atmosphere. Additional optional states can be configured to track correlated sensor errors such as sensor biases and sensor axis misalignment errors. The base state vector is defined as follows:

$$\mathbf{x} = \begin{bmatrix} u & v & w & r & \phi & \theta & \mathbf{q} & \mathbf{w}_{ned} & p_\infty & d_\infty \end{bmatrix}^T \tag{1}$$

where $u$, $v$, and $w$ are the three components of the inertial velocity vector in a geocentric coordinate frame in which the z-axis is directed towards the center of the planet along the radius vector, the y-axis it to the east, and the x-axis is perpendicular to the radius vector in a northerly direction. The radius $r$ is the distance of the vehicle from the center of the planet. The angles $\phi$ and $\theta$ are the declination and longitude in radians, respectively. These coordinates are with respect to the planetary body at which the vehicle is arriving at, which we refer to as the *target body*. These coordinates are in a Planet-Centered Planet-Fixed (PCPF) frame, where *planet* can refer to a planet, or another type of planetary body such as a moon or astroid. The quaternion $\mathbf{q}$ contains the coordinate transformation from the local North-East-Down (NED) frame to the body frame. The wind vector $\mathbf{w}_{ned}$ contains the atmospheric winds along the trajectory, in the NED frame. Finally, $p_\infty$ and $d_\infty$ contain the static pressure and density of the atmosphere around the vehicle.

The kinematic states of the state vector are governed by the kinematic equations of motion and the atmospheric states are governed by atmospheric equations of motion based on the hydrostatic equation and the ideal gas law [6]. The wind states are modeled as a random walk process where $\dot{\mathbf{w}}_{ned} = 0$.

The angular velocities and specific forces driving the kinematic equations of motion are obtained from the input vector $\mathbf{u}$, where the source of these inputs are the specific force measurements $\mathbf{f}$ from an accelerometer and the angular velocity measurements $\boldsymbol{\omega}$ from a gyroscope such that the measurement vector is

$$\mathbf{u}_k = \begin{bmatrix} \boldsymbol{\omega}_k & \mathbf{f}_k \end{bmatrix}^T \tag{2}$$

In reality, these inertial measurements are corrupted by white noise, biases, scale factor errors, and sensor misalignment errors. Error sources that can be approximated as zero mean Gaussian, such as additive white noise, can be handled statistically within the Kalman filtering framework. Correlated error sources, such as biases and scale factor errors, can be configured in the NewSTEP configuration files and estimated as additional states in the NewSTEP state vector.

# 3 Doppler Tracking Measurement Model

In a state estimation filter, the measurement model $\mathbf{y} = z(\mathbf{x})$ relates the state vector $\mathbf{x}$ to the measurement vector $\mathbf{y}$. In the case of the Doppler tracking measurement model, the only element in the measurement vector is the frequency of the radio signal measured by the receiving antenna. We will denote this frequency as $f_r$ such that

$$\mathbf{y} = \begin{bmatrix} f_r \end{bmatrix} \tag{3}$$

For this work, we assume that the receiving antenna is located on Earth and its precise position on Earth is known. The received frequency $f_r$ is related to the transmitted frequency $f_0$ by the following relation [9]:

$$f_r = \frac{f_0(c + \dot{d})}{c} + f_{cal} \tag{4}$$

where $c$ is the speed of light and $\dot{d}$ is the time derivative of the distance $d$ between the receiving telescope and the spacecraft. The last term, $f_{cal}$, includes effects on the frequency due to general relativity, special relativity, and atmospheric refraction.

To calculate the expected value of $\dot{d}$ for a vehicle with a state vector of $\mathbf{x}$, we must consider the position and velocities of the spacecraft, planetary body, and receiving telescope in an inertial reference frame, as well as the time delay for the signal to travel from the transmitter to the receiving telescope.

Generally, either the transmission time, denoted by $t_0$, or the reception time, denoted by $t_r$, of the radio signal is known. If the reception time is available and some general information about the positions of the spacecraft and the receiver are known, the transmission time can be calculated using the known speed of light. The same is true for calculating the reception time if given the transmission time. The time delay, denoted by $\Delta t$, and the transmission or reception time can be calculated as follows:

$$\Delta t = dc \tag{5}$$

$$t_r = t_0 + \Delta t \tag{6}$$

$$t_0 = t_r - \Delta t \tag{7}$$

We denote the position vector of the Earth in the inertial frame as $\mathbf{p}_e^i(t)$, the inertial velocity vector of Earth as $\mathbf{v}_e^i(t)$, the position vector of the target body in the inertial frame as $\mathbf{p}_t^i(t)$, and the inertial velocity vector of the target body as $\mathbf{v}_t^i(t)$. All of these positions and velocities are functions of time. Both of the position vectors should have the same origin, such as the solar system barycenter. This way, the difference between the two positions results in the relative position between the two bodies. The relative velocity between the two bodies can also be found by calculating the difference between the two velocity vectors, provided that both of the velocity vectors are in the same inertial reference frame.

The position of the receiving telescope in the Earth-centered Earth-fixed (ECEF) frame (rotating frame) is denoted as $\mathbf{p}_r^{\text{ECEF}}$. This position is a known constant of

the system. We assume that the position of the receiving telescope is constant and has a velocity of zero in the planet-fixed frame. The transformation matrix that transforms this non-inertial position to the inertial frame as a function of time is defined as $\mathbf{T}^i_{\text{ECEF}}(t)$ such that the position of the receiver in the Earth-centered inertial frame $\mathbf{p}^i_r$ and velocity of the receiver in the Earth-centered inertial frame $\mathbf{v}^i_r$ are

$$\begin{bmatrix}\mathbf{p}^i_r(t)\\ \mathbf{v}^i_r(t)\end{bmatrix} = \mathbf{T}^i_{\text{ECEF}}(t)\begin{bmatrix}\mathbf{p}^{\text{ECEF}}_r\\ \boldsymbol{\omega}_e \times \mathbf{p}^{\text{ECEF}}_r\end{bmatrix} \tag{8}$$

where $\boldsymbol{\omega}_e$ is the Earth's angular velocity.

The position and velocity of the spacecraft relative to the target body are unknown quantities in the system. Therefore, estimates of $r$, $\phi$, $\theta$, $u$, $v$, and $w$ are parameters in the measurement model. In order to transform the latitudinal position frame and the local inertial NED velocity frame used by the NewSTEP state vector to the Cartesian inertial reference frame, we first transform the position and velocity to an intermediary rectangular PCPF frame. The position and velocity vectors in the NewSTEP frame are converted to the PCPF rectangular frame as follows:

$$\dot{r} = -w \tag{9}$$

$$\dot{\phi} = \frac{u}{r} \tag{10}$$

$$\dot{\theta} = \frac{v}{\cos(\phi)r} - \omega_p \tag{11}$$

$$\mathbf{p}^{\text{PCPF}}_s = \begin{bmatrix}\cos(\phi)\cos(\theta)\\ \cos(\phi)\sin(\theta)\\ \sin(\phi)\end{bmatrix} r \tag{12}$$

$$\mathbf{v}^{\text{PCPF}}_s = \begin{bmatrix}\cos(\phi)\cos(\theta) & -\sin(\theta) & -\sin(\phi)\cos(\theta)\\ \cos(\phi)\sin(\theta) & \cos(\theta) & -\sin(\phi)\sin(\theta)\\ \sin(\phi) & 0 & \cos(\phi)\end{bmatrix}\begin{bmatrix}\dot{r}\\ r\dot{\theta}\cos(\phi)\\ r\dot{\phi}\end{bmatrix} \tag{13}$$

where $\mathbf{p}^{\text{PCPF}}_s$ is the position of the spacecraft in the rotating PCPF frame, and $\mathbf{v}^{\text{PCPF}}_s$ is the velocity of the spacecraft in the rotating PCPF frame.

Next, the transformation matrix $\mathbf{T}^i_{\text{PCPF}}(t)$ transforms the position and velocity from the PCPF frame to the planet-centered inertial frame such that the position of the spacecraft in the inertial frame $\mathbf{p}^i_s$ and the velocity of the spacecraft in the inertial frame $\mathbf{v}^i_s$ are

$$\begin{bmatrix}\mathbf{p}^i_s(t)\\ \mathbf{v}^i_s(t)\end{bmatrix} = \mathbf{T}^i_{\text{PCPF}}(t)\begin{bmatrix}\mathbf{p}^{\text{PCPF}}_s\\ \mathbf{v}^{\text{PCPF}}_s\end{bmatrix} \tag{14}$$

Figure 2 shows the ECEF and PCPF references and their relation to the inertial frame. Figure 3 how to decompose from PCPF coordinate frame to NED coordinate frame.

The tool we used to calculate $\mathbf{p}^{\mathbf{i}}_{\mathbf{e}}(\mathbf{t})$, $\mathbf{v}^i_e(t)$, $\mathbf{p}^i_t(t)$, $\mathbf{v}^i_t(t)$, $\mathbf{T}^i_{\text{ECEF}}(t)$, and $\mathbf{T}^i_{\text{PCPF}}(t)$ is the Spacecraft, Planet, Instrument, C-Matrix, Events (SPICE) toolkit developed by NASA's Navigation and Ancillary Information Facility (NAIF) and the

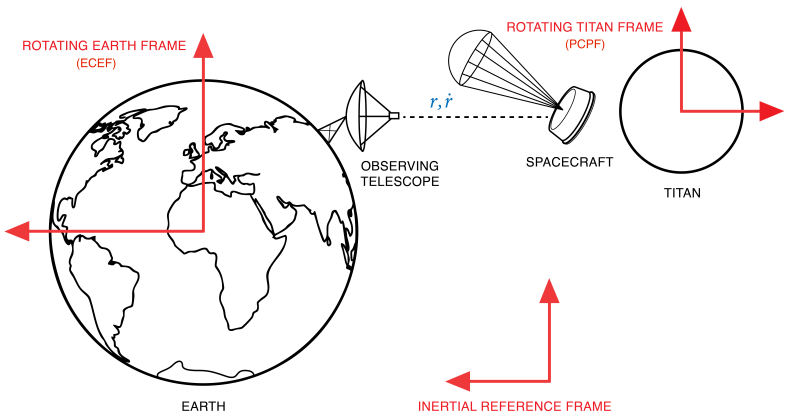


**Figure 2: Coordinate systems on Earth and Titan that are relevant for the Doppler tracking problem.**

Jet Propulsion Laboratory (JPL). The SPICE toolkit[1] is a library of functions to compute parameters related to the observations at specified times [10–12]. These parameters include positions, velocities, and orientations of planets, satellites, comets, asteroids, and spacecraft. JPL and NAIF also maintain a comprehensive library of SPICE kernel files, containing ephemeris data and frame definitions for various planets and their satellites. A SPICE Matlab application programming interface (API) known as MICE[2] is also available. The MICE API was used in this work to implement the SPICE data kernels and coordinate transformation routines.

Once all of the necessary transformations have been performed, simple vector algebra is used to calculate the range rate $\dot{d}$ between the satellite and the receiving telescope.

$$\mathbf{p}_{rel} = (\mathbf{p}_e^i(t_r) + \mathbf{p}_r^i(t_r)) - (\mathbf{p}_s^i(t_0) + \mathbf{p}_t^i(t_0)) \tag{15}$$

$$\mathbf{v}_{rel} = (\mathbf{v}_e^i(t_r) + \mathbf{v}_r^i(t_r)) - (\mathbf{v}_s^i(t_0) + \mathbf{v}_t^i(t_0)) \tag{16}$$

$$d = ||\mathbf{p}_{rel}||_2 \tag{17}$$

$$\dot{d} = \left\langle \mathbf{v}_{rel}, \frac{\mathbf{p}_{rel}}{d} \right\rangle \tag{18}$$

The last remaining component of the Doppler shift is the relativistic affects $f_{cal}$. The physics to calculate the atmospheric effects and relativistic effects is out of the scope of this work, and we point the interested reader to [13] for more information on the effects of general relativity, [14] for more information on special relativity, and [15] for more information on the effects of atmospheric density on a signal's Doppler shift. In this work, we treat $f_{cal}$ as a calibration constant which we use to configure the measurement model. More information on this process can be found in Section 4.2.2.

[1] https://naif.jpl.nasa.gov/naif/toolkit.html, accessed July 2025.
[2] https://naif.jpl.nasa.gov/naif/toolkit_MATLAB.html, accessed July 2025.

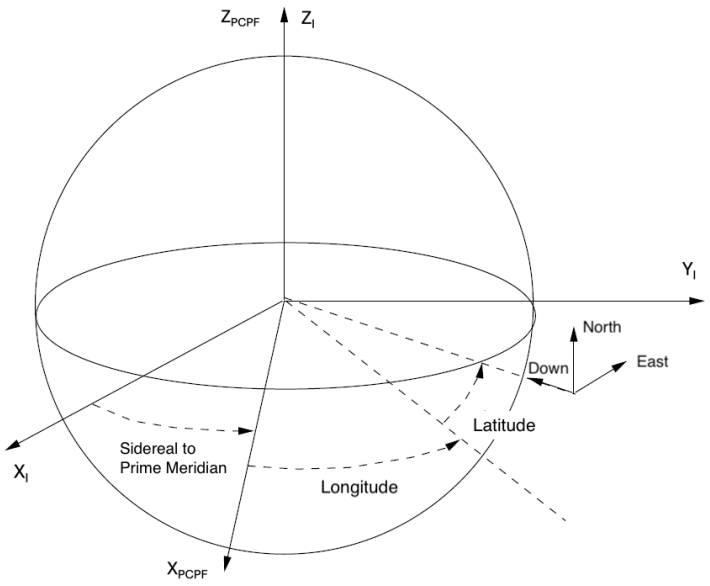


**Figure 3: Relationship between inertial, planet center planet fixed (PCPF), and north, east, down (NED) frames.**

The final frequency calculation presented below completes the Doppler shift measurement model.

$$\mathbf{y} = f_r = h(\mathbf{x}) = \frac{f_0(c + \dot{d})}{c} + f_{cal} \tag{19}$$

Whenever necessary for the IEKF, the measurement model $h(\mathbf{x})$ is linearized numerically using the finite difference method.

# 4 Case Studies

The Doppler tracking model described in Section 3 was implemented into NewSTEP, and was tested using two Titan entry, descent, and landing case studies. The first case study was a simulation of the Huygens probe, which traveled with the Cassini spacecraft to Titan and landed on the surface in January of 2005. The second case study uses flight data, collected as part of the Huygens Doppler Wind Experiment. This flight data includes Doppler shifts from communication equipment onboard the Huygens spacecraft transmitted from Huygens at Titan and received at Earth during the Huygens descent phase. For both of these scenarios, NewSTEP was configured as an Iterative Extended Kalman Filter, and no smoothing was performed by NewSTEP.

## 4.1 Case Study 1: Simulated Data of Huygens Entry, Descent, and Landing

### 4.1.1 Data for Case Study 1

The goal of the first case study is to test the measurement model developed in the last section with data where the truth is known. The simulated data was used in this work was generated using a Huygens EDL modeling and simulation in Program to Optimize Simulated Trajectories II (POST2) [16]. The simulation used best practices based on some recent flight projects and improvements [17,18]. POST2 is a generalized point mass, discrete parameter targeting and optimization program. The simulation used is a six degree-of-freedom trajectory beginning at an altitude of 1270 kilometers above the surface of Titan and ending shortly before touchdown. The simulated trajectory is meant to resemble the trajectory flown by the Huygens probe. The simulated trajectory is shown in Figure 4. This trajectory includes entry interface, pilot parachute deployment, main parachute deployment, drogue parachute deployment, and approximately two and a half hours of flight under the drogue parachute as the vehicle is descending towards the surface of Titan. A timeline of events along the POST2 simulated trajectory is listed in Table 1.

**Table 1: Simulation timeline of events.**

| Event | Time (min) |
|---|---|
| Entry Interface (1270 km) | 0.0 |
| Main Parachute Deploy | 4.54 |
| Stabilizer Deploy | 19.5 |
| Touchdown | 156.6 |

Based on the simulated trajectory, the following sensors were simulated for the entry vehicle: an accelerometer triad, a gyroscope triad, a static pressure sensor, and a static temperature sensor. Additionally, Doppler measurements were made available from POST2 to simulate communications between the Huygens probe and the radio telescope at Parkes Observatory in Australia. The sensors were corrupted by zero-mean Gaussian noise, with the noise statistics presented in Table 2. Note, this measurement suite is not representative of the actual Huygens payload, but more akin to modern EDL planetary flights.

**Table 2: Error characteristics for the simulated Huygens sensors.**

| Sensor | $1\sigma$ error bound |
|---|---|
| Accelerometer Triad | 70 micro g ($1g = 9.81m/s$) |
| Gyroscope Triad | 1/3600 deg/sec |
| Pressure Sensor | 1 Pa (t=0 sec to t= 2000 sec), |
| | 100 Pa (t=2000 sec to t=9400 sec) |
| Temperature Sensor | 0.25 K |
| Doppler Measurements | 1 Hz |

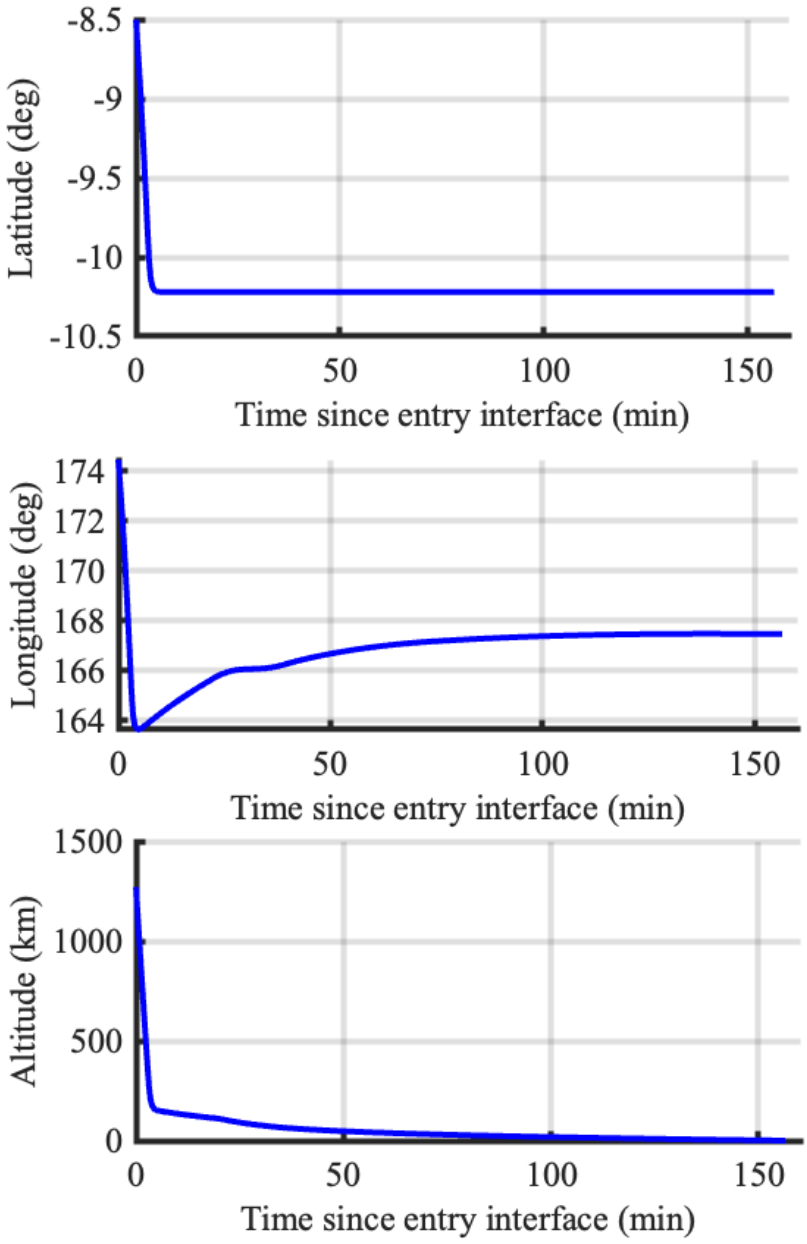


**Figure 4: Huygens simulation flight trajectory based on Ref [16].**

The IEKF was initialized using the position, velocity, attitude, atmospheric pressure, and atmospheric density from the simulator at the beginning of the trajectory. A small amount of error, based on data from other flight projects, was added to the initial conditions. The error was assumed to be zero-mean Gaussian noise, with the noise statistics presented in Table 3.

**Table 3: Error characteristics for the initial conditions of the IEKF during the simulated Huygens trajectory.**

| Initial Condition | Gaussian $1\sigma$ error bound |
|---|---|
| Altitude | 50 m |
| North-South Position | 50 m |
| East-West Position | 50 m |
| Descent Rate | 5 m/s |
| Meridional Velocity | 5 m/s |
| Zonal Velocity | 5 m/s |
| Yaw | 0.5 degrees |
| Pitch | 0.5 degrees |
| Roll | 0.5 degrees |
| Atmospheric Pressure | 0.01 % error |
| Atmospheric Density | 0.01 % error |

Lastly, the SPICE kernels that were used for the analysis described in this report are listed in Table 4. These kernels provide various data required to define coordinate frames, orbits, physical constants of celestial bodies, and coordinates of Earth-based tracking stations. The specific PCPF frames defined by the SPICE kernels relevant to this problem are the International Terrestrial Reference Frame of 1993 (ITRF93), describing the orientation of the Earth, and the International Astronomical Union (IAU) coordinate frame for Titan (IAU_TITAN).

**Table 4: SPICE kernels used for the reconstruction. All kernels accessed July 2025.**

| Kernel | Description |
|---|---|
| naif0012.tls | Leap seconds |
| 050214_PE_DE405.BSP | Orbits of planets |
| gm_de431.tpc | Mass parameters of planets and satellites |
| ndosl_190716_v02.bsp | WGS-84 directory of station locations |
| pck.sat441_IAU2009Frame.tpc | Planetary constants for Saturn and moons |
| SAT199.BSP | Orbits of Saturn's moons |
| earthstns_fx_050714.bsp | DSN station locations data |
| earthstns_fx_050714.cmt | DSN station locations comments |
| pck00010.tpc | Planetary coordinate frame definitions |
| earth_620120_240827.bpc | Earth orientation data |

In this case study, two scenarios were examined and compared. In the first scenario, the trajectory reconstruction was performed using only the accelerometer triad, the gyroscope triad, the pressure sensor, and the temperature sensor. In the second scenario, the Doppler measurements were also included with the previous sensors. The purpose of this comparison was to quantify the improvement of the Doppler measurements on the trajectory reconstruction.

### 4.1.2 Results of Case Study 1

The position and velocity errors in the reconstruction, using only the accelerometer triad, the gyroscope triad, the pressure sensor, and the temperature sensor, are shown in Figures 5 and 6. These errors were calculated by subtracting the reconstructed position and velocity from the positions and velocities given by the POST2 simulation, which were treated as the ground truth. These position and velocity errors are presented in the local NED frame. The $3\sigma$ bounds on the plots are based on the covariance estimates produced by the IEKF. One can see the large position and velocity standard deviations when Doppler data is not used in the reconstruction and solely IMU data is used for reconstruction.

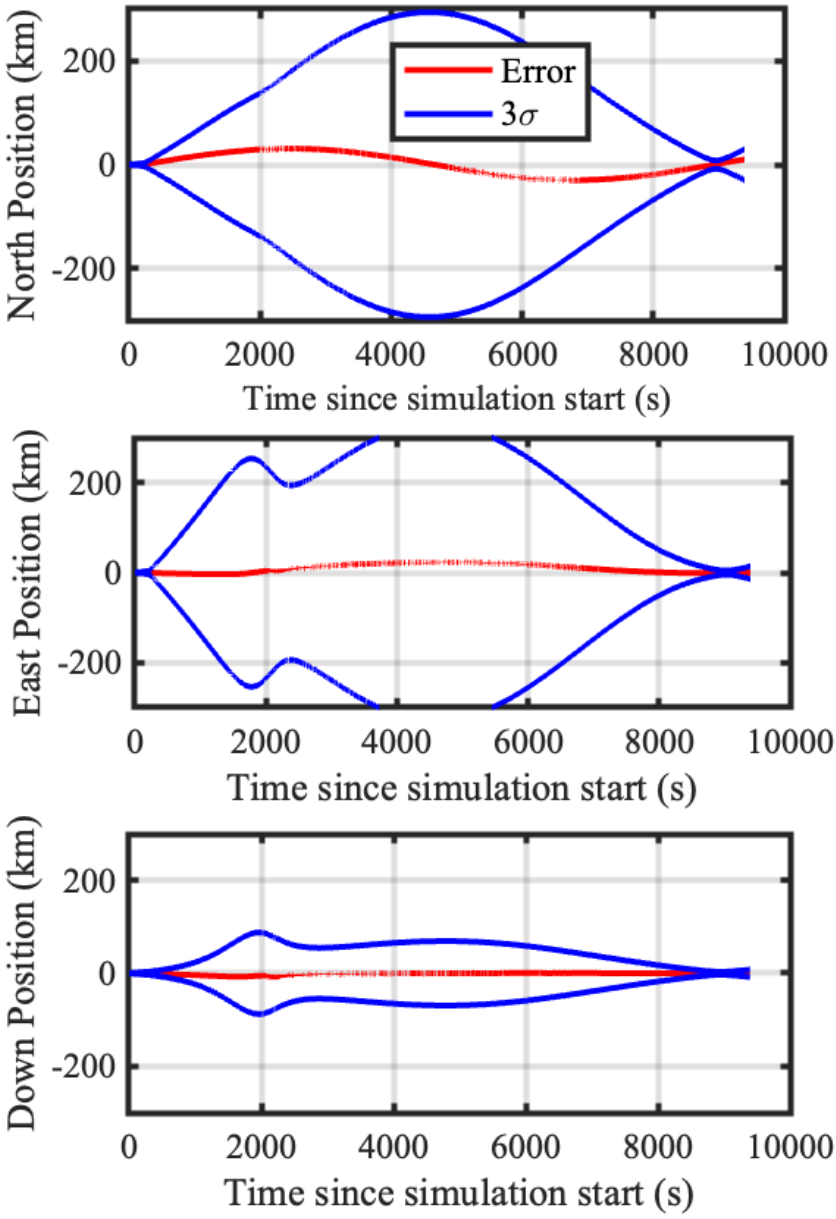


**Figure 5: Estimate errors from reconstruction of Huygens simulated position without Doppler measurements.**

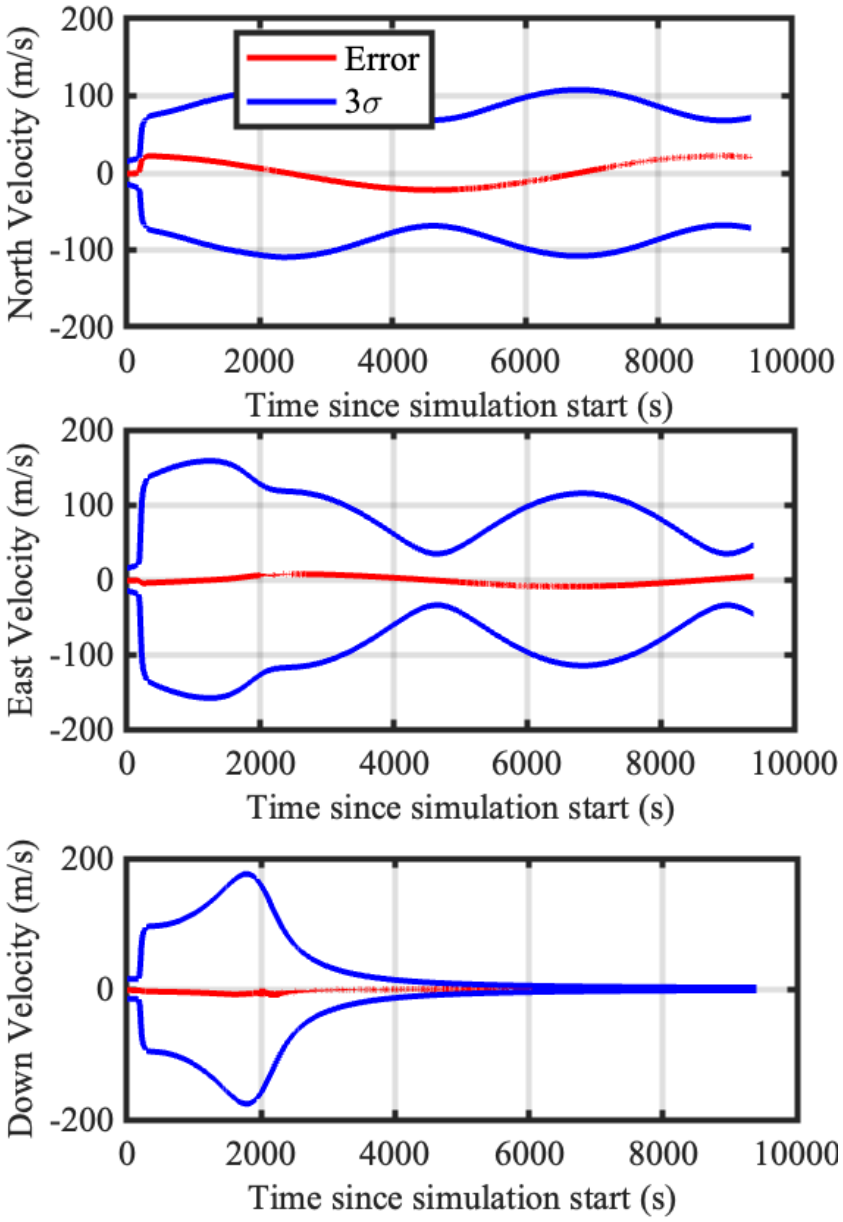


**Figure 6: Estimate errors from reconstruction of Huygens simulated velocity without Doppler measurements.**

Figures 7 and 8 show similar position and velocity errors for the trajectory reconstruction that included the Doppler measurements. These errors were also calculated by subtracting the reconstructed position and velocity from the simulated position and velocity, and are presented in the NED frame.

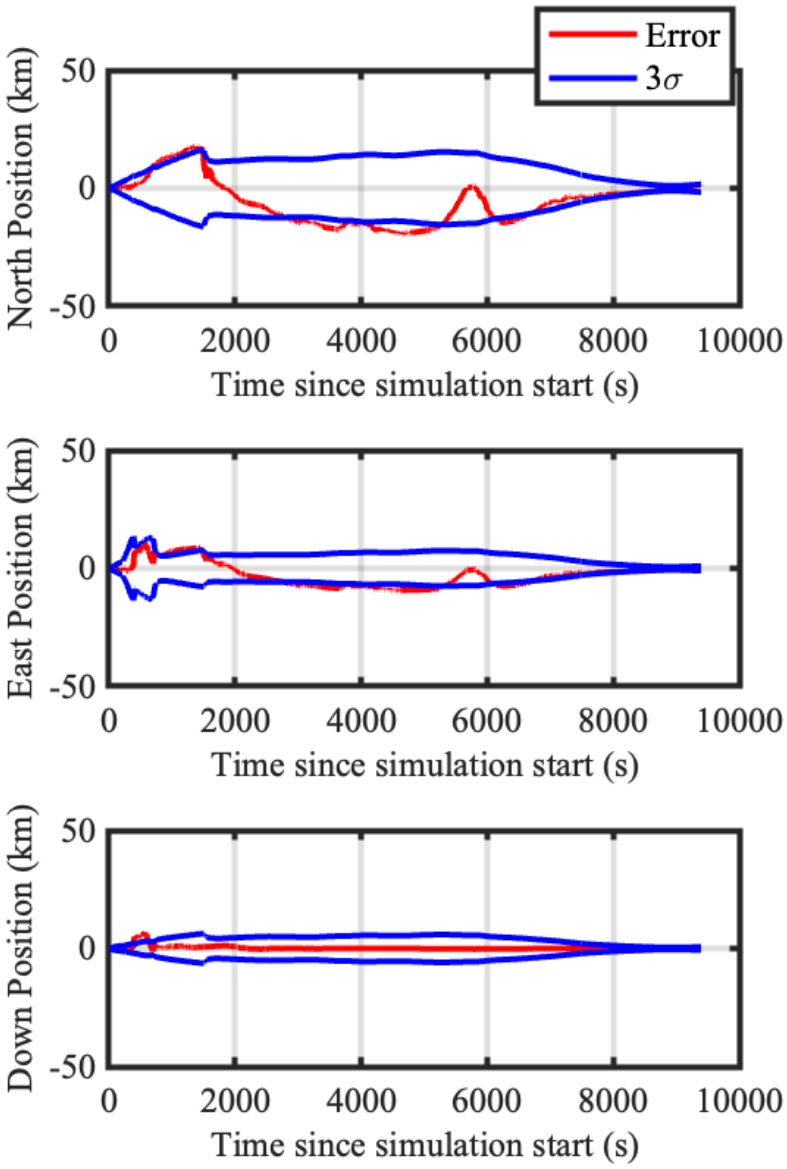


**Figure 7: Estimate errors from reconstruction of Huygens simulated position with Doppler measurements.**

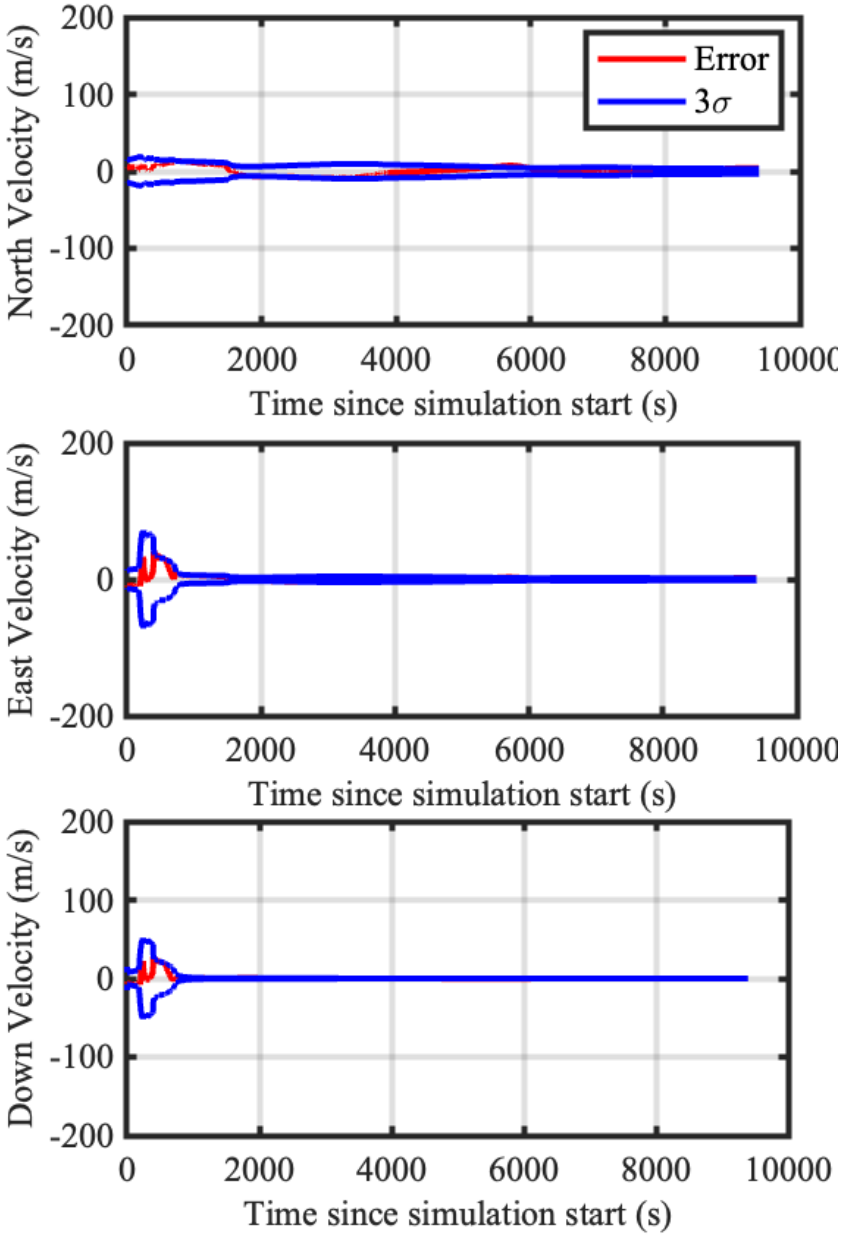


**Figure 8: Estimate errors from reconstruction of Huygens simulated velocity with Doppler measurements.**

It is clear from these figures that the inclusion of the Doppler measurements significantly improved the accuracy of the trajectory reconstruction. The root mean square of the $3\sigma$ bound on the position error during the trajectory improved from 285.940 km without the Doppler measurements to 1.375 km with the Doppler measurements, and the root mean square of the $1\sigma$ position error bound improved from 9.531 km without Doppler measurements to 0.458 km with Doppler measurements.

The root mean square of the $3\sigma$ bound on the velocity error magnitude improved from 149 m/s without the Doppler measurements to 14.3 m/s with the Doppler measurements, and the root mean square of the $1\sigma$ velocity error magnitude bound improved from 50 m/s without Doppler measurements to 4.8 m/s with Doppler measurements. The North-South velocity, East-West velocity, and vertical velocity saw 91%, 94%, and 96% improvements, respectively. The North-South position, East-West position, and vertical position saw 93%, 97%, and 91% improvements, respectively.

The improvements in the positions and velocities in the East-West direction appear to be more significant than the improvements in the velocities in the North-South direction. This is because the position and orientation of the planets on the ecliptic plane tend to require that radio communications from Huygens travel in the East-West direction towards Earth. This leads to better observability for these modes of the position and velocity. However, when a high-quality three-axis accelerometer and gyroscope are available, the Doppler shift measurements can also improve the North-South position and velocity estimates because of the correlations between the north-south and east-west state estimate errors that are tracked by the IEKF.

## 4.2 Case Study 2: Flight Test Data from the Huygens Doppler Wind Experiment

### 4.2.1 Data for Case Study 2

One of the experiments flown on the Huygens probe was the Doppler Wind Experiment [19, 20]. The goal of the Doppler Wind Experiment was to estimate the zonal winds in Titan's atmosphere during descent by analyzing the Doppler shift in a signal transmitted by the Doppler winds experimental package on the Huygens descent probe. In the Doppler Winds Experiment, the original plan was to have the Doppler shifts measured by the Cassini orbiter to determine the Doppler winds. Unfortunately, the data from the Cassini orbiter was not recovered; however, radio telescopes on Earth at Parkes (Australia) Observatory and Green Bank (West Virginia, US) Observatory were able to measure the Doppler shifts from Huygens' transmissions. In this second case study, we use these Doppler shifts to estimate the velocity of the Huygens probe as it was descending towards the surface of Titan.

We begin the reconstruction at an altitude of 144 km above the surface of Titan, which is when the first Doppler wind measurements are available from the Green Bank telescope. This happens approximately 10 seconds after the main parachute is deployed and approximately 15 minutes before parachute exchange (the main parachute is released and the drogue/stabilizer parachute is deployed). We end the reconstruction approximately 90 minutes later when the signal from the Green Bank Telescope is lost. This occurs at an altitude of approximately 13 kilometers above the surface of Titan. Several minutes later, shortly before the spacecraft reaches the surface, the Parkes Telescope acquires the Huygens transmission. The lock by the Parkes telescope continues for several hours after Huygens has touched down and is sitting on the surface. In this work, we only used the Doppler measurements from

Green Bank Telescope for the trajectory reconstruction; however, the data from the Parkes Telescope was used for the calibration of the measurement.

Unlike the simulated vehicle studied in Section 4.1, the Huygens probe did not have an onboard gyroscope, as at the time that Huygens was designed, there were no solid-state gyroscopes that were qualified for space flight [21]. Instead, the Huygens probe used an accelerometer that was offset from the body axis of rotation and oriented in the radial direction to measure the centripetal force. The centripetal force could then be used to estimate the magnitude of the angular velocity about the vehicle spin axis. Huygens did have a 3-axis accelerometer triad, but the two horizontal body-axis accelerometers were not transmitting telemetry after the parachute deployment to preserve the communication bandwidth for other experiments [22, 23]. For this reason, we chose to track only the vehicle's position for this case study. We assume the attitude of Huygens to be constant, under the parachute as it descends. We enforce this in the IEKF by setting the attitude rates of change in the filter time update to be zero, and ensure that attitude estimate covariance remains at zero. This causes the attitude states in the filter to effectively be ignored.

The vertical velocity and altitude states are driven by the vertical-axis accelerometer, for which measurements are available during the entire atmospheric entry, descent, and landing. However, since no horizontal-axis accelerometer data was available during the portion of the flight we wished to reconstruct, we assumed the horizontal specific forces to have a mean of zero. We included a large uncertainty of 50 $\mathrm{m/s^2}$ on these specific forces in the IEKF process model to account for unmeasured dynamics.

It should be noted that including states with poor observability in the IEKF caused the covariances between states to grow extremely large. In an effort to prevent numerical instability, we periodically cleared the correlations in the filter and continued the trajectory reconstruction with a fresh, uncorrelated state estimate.

We initialize our estimator with initial conditions provided by the Huygens Descent Trajectory Working Group (DTWG) [24]. The initial position and velocity is listed in Table 5. Additional data products used in the reconstruction can be found in the Planetary Data System (PDS) archive at locations provided in Table 6. A timeline of events along the Huygens trajectory after 144 km altitude is listed in Table 7. The planned Huygens concept of operations is shown in Figure 9. The pilot parachute and main parachute are all deployed prior to 144 km altitude, with heatshield separation occurring before the start of the reconstruction efforts here.

**Table 5: Initial conditions of the IEKF.**

| Initial Condition | Value |
|---|---|
| $u$ | 3.900 m/s |
| $v$ | 110.207 m/s |
| $w$ | 51.394 m/s |
| $r$ | 2719.036 km |
| $\phi$ | -10.326 deg |
| $\theta$ | 164.060 deg |
| $\mathbf{w}_{ned}(1)$ | 0 m/s |
| $\mathbf{w}_{ned}(2)$ | 0 m/s |
| $\mathbf{w}_{ned}(3)$ | 0 m/s |
| $p_\infty$ | 294 Pa |
| $d_\infty$ | 0.006255 kg/m$^3$ |

**Table 6: Huygens PDS archive data products. All link paths are provided relative to https://atmos.nmsu.edu/PDS/data. All data products accessed July 2025.**

| Data Product | PDS Archive Location |
|---|---|
| DWE Data | /PDS4/Huygens/hpdwe_bundle/DATA/ |
| DTWG Sensor Data | /PDS4/Huygens/hpdtwg_bundle/EXTRAS/ |
| DWE Trajectory | /PDS4/Huygens/hpdwe_bundle/GEOMETRY/ |
| DTWG Trajectory | /PDS4/Huygens/hpdtwg_bundle/DATA/ |
| Houskeeping Data | /hphk_0001/DATA/ |

**Table 7: Huygens trajectory timeline of events[3]**

| Event | Time since 144 km altitude (min) |
|---|---|
| Entry Interface (1270 km) | -7.3 |
| Pilot Parachute Deploy | -1.48 |
| Main Parachute Deploy | -1.42 |
| Heatshield Separation | -0.958 |
| 144 km altitude | 0.0 |
| Stabilizer Deploy | 13.5 |
| Start of Doppler Data Gap | 105.24 |
| End of Doppler Data Gap | 131.7 |
| Touchdown | 146.9 |

The Doppler residual data to the Green Bank observatory was used in this work. Figure 10 shows the data used for the trajectory reconstruction. One can see the gap in the Doppler data between 130 and 140 min after main parachute deployment. This gap of data will affect the reconstruction results shown in the next section.

[3]https://pds-atmospheres.nmsu.edu/data_and_services/atmospheres_data/Huygens/extras/KeyEvents-3.htm, accessed August 2025.

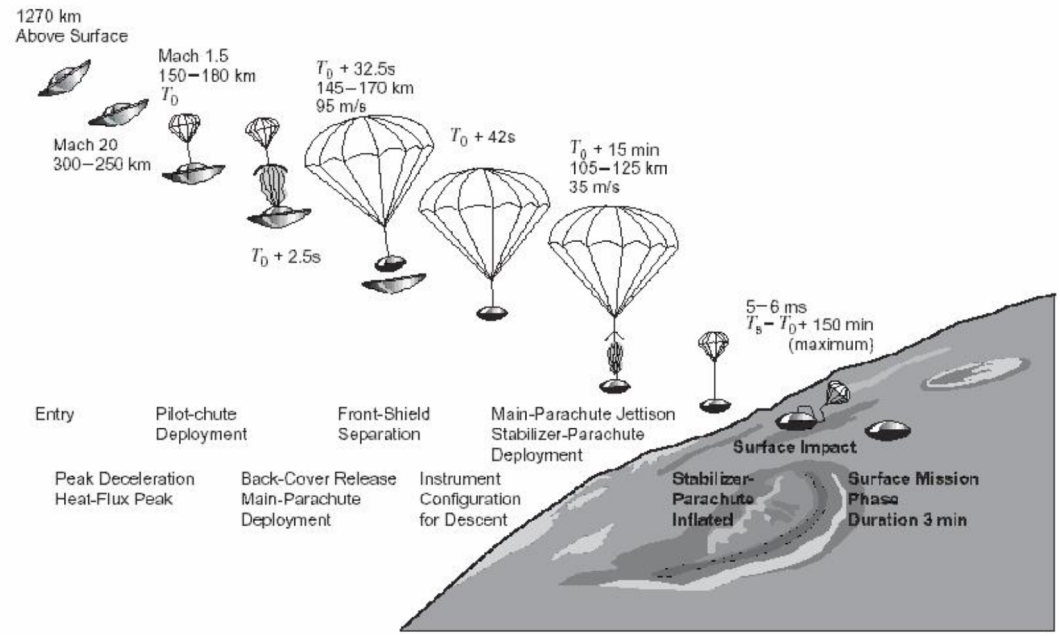


**Figure 9: Concept of operations of the Huygens mission (figure reproduced from [25]).**

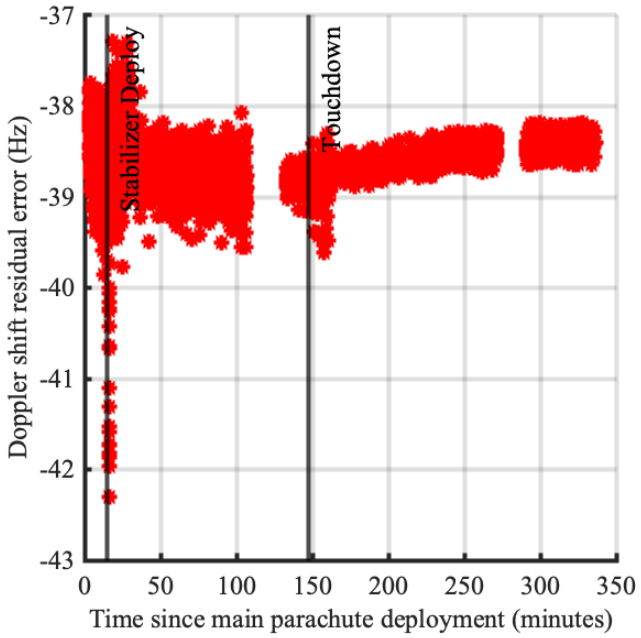


**Figure 10: Doppler Shift Residual from Huygens to Green Bank Observatory.**

### 4.2.2 Doppler Calibration of Case Study 2

After Huygens landed on the surface of Titan, the Doppler Winds Experiment continued to operate and transmit radio signals. Although most of the communications with Huygens ended 72 minutes after touchdown, when Huygens and Cassini lost line of sight around the horizon of Titan and Cassini could no longer relay communications, the Doppler wind experiment remained unaffected because its radio transmissions traveled directly to Earth [26]. There are approximately three hours of data collected from the Parkes Telescope while the Huygens probe was on the surface of Titan. This data can be used to calibrate the estimator and correct for any effects from special relativity, general relativity, and atmospheric refraction.

This calibration relies on the assumption that the vehicle is stationary while it is sitting on the surface such that the components of Huygens' NewSTEP inertial velocity vector are $u = 0$, $w = 0$, and $v$ is the inertial velocity of Huygens from only the rotation of Titan. We also must have an estimate of the position of Huygens on the surface of Titan. In this case, we have this surface position available from the Huygens DTWG, listed in Table 8. All of the other components of the relative velocity can be calculated with knowledge of the transmission time of the signal and the position of Huygens on the surface of Titan. If we let $\mathbf{x}_{surface}$ be the state of Huygens on the surface of Titan and we define $f_{surface}(t)$ to be the time history of the frequency measured by the receiving telescope for messages transmitted while Huygens was on the surface, we can initially set $f_{cal} = 0$ to calculate the following measurement residuals:

$$\delta y(t) = y(x_{surface}) - f_{surface}(t) \tag{20}$$

**Table 8: Position of Huygens on the surface of Titan.**

| Position | Value |
|---|---|
| $r$ | 2575 km |
| $\phi$ | -10.251 deg |
| $\theta$ | 167.686 deg |

Next, we must find $f_{cal}$ such that the absolute value of $\delta y(t)$ is minimized. In Figure 11, we plot $\delta y(t)$ for the portion of the Doppler data where Huygens is on the surface. We can see from inspection that there is bias in $\delta y(t)$ of around -38.5 Hz. For this work, we corrected for this bias by setting a constant value of $f_{cal} = 38.5$ Hz.

The other necessary assumption is that the the systematic errors we wish to eliminate through calibration remain constant over the duration of the trajectory reconstruction.

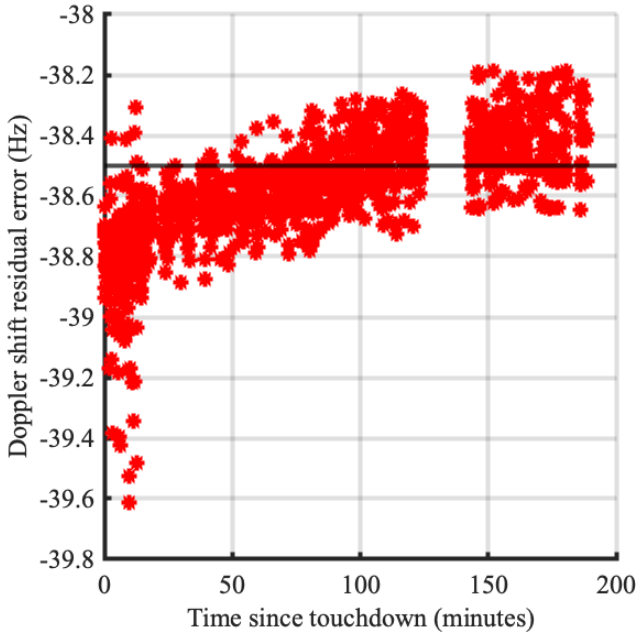


**Figure 11: Doppler shift measurement residuals at the Parkes Observatory while Huygens is on the surface of Titan.**

### 4.2.3 Results of Case Study 2

Figures 12-13 show a comparison of the position and velocity published by the DTWG and the reconstruction from the Doppler measurements. The DTWG's trajectory was created using temperature measurements, pressure sensors, molecular mass measurements, zonal wind measurements, and image-based drift measurements from a downwards-facing camera mounted on the probe. The NewSTEP trajectory used only Doppler measurements, temperature measurements, pressure measurements, and the vertical-axis accelerometer for the reconstruction. With only Doppler measurements available to measure lateral velocity, the velocity reconstruction errors were much larger and were not able to produce a reasonable position estimate. However, the results show that the Doppler measurements allowed the estimator to successfully track the velocity of the vehicle, especially in the east-west direction, due to the geometry of spacecraft relative to the Earth-based Doppler observation. Without access to measurements from a gyroscope or an accelerometer measuring specific forces in the in the horizontal direction, the north-south velocities and latitudinal position contained much more uncertainty.

Shown in Figure 14 are the $1\sigma$ error bounds from the velocity reconstruction. Although these $1\sigma$ bounds are much more conservative than the error bounds calculated in Case Study 1 due to the need to inflate the variances of the accelerometer sensors, it is clear that the estimate of the velocity in the east direction is more accurate than the estimate of the velocity in the north direction. Again, this is because the radio signals must travel in Titan's east-west direction to get to from Huygens to Earth, causing greater observability for this mode of the velocity.

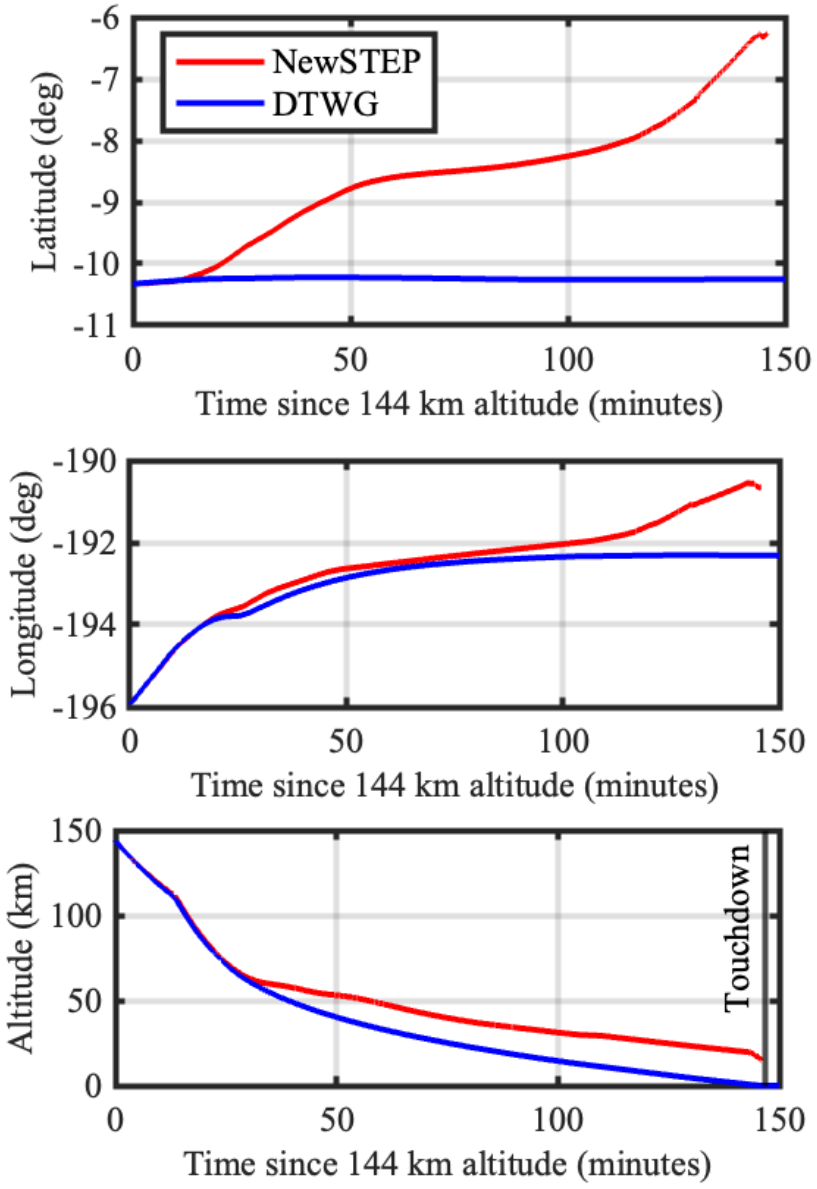


**Figure 12: Comparison of position published by the Huygens DTWG with the position vector estimated using the Doppler measurements**

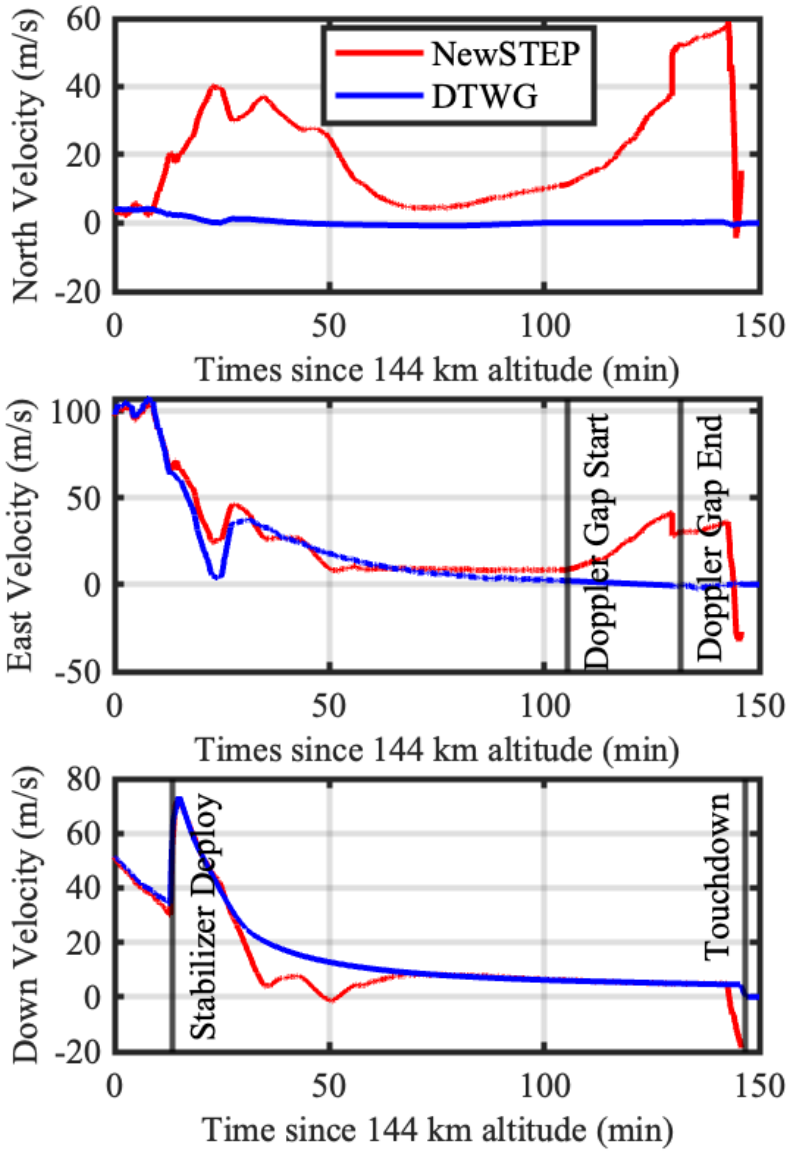


**Figure 13: Comparison of velocity published by the Huygens DTWG with the velocity estimated using the Doppler measurements.**

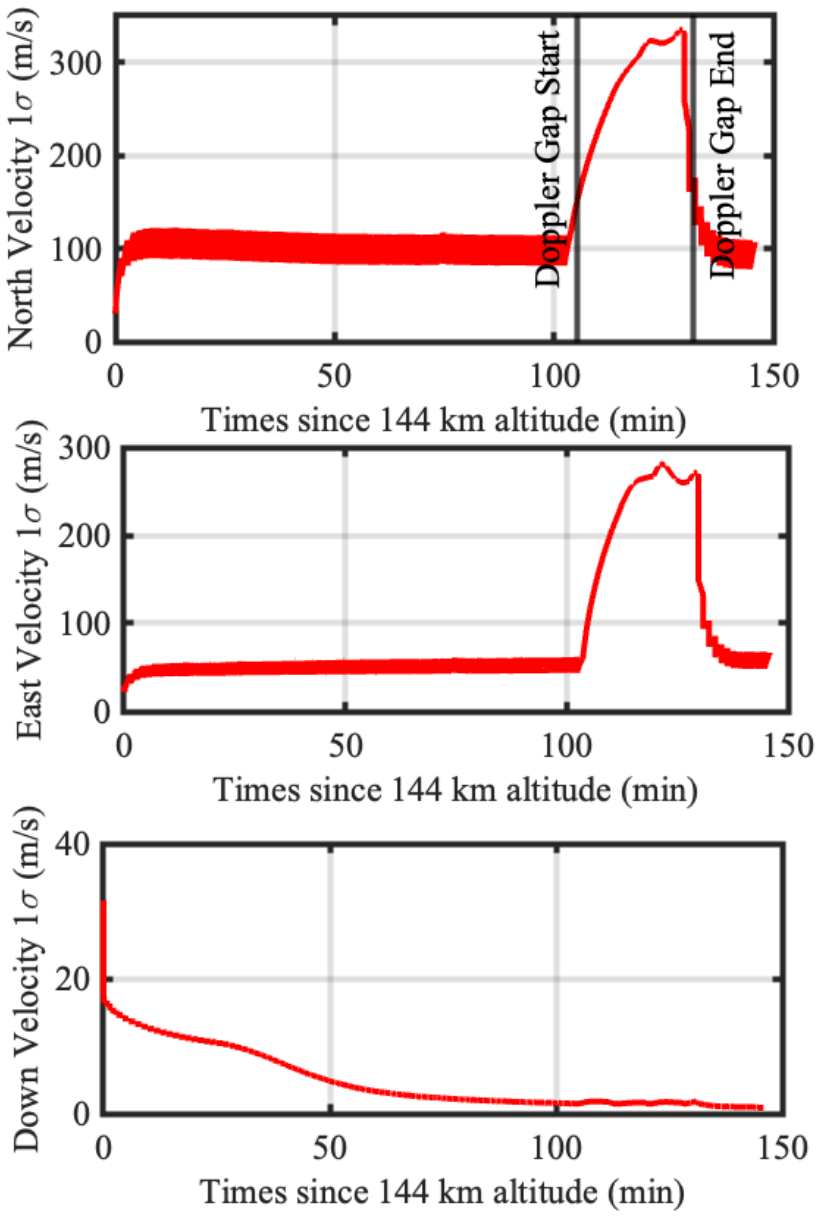


**Figure 14: The $1\sigma$ error bounds of the Huygens velocity reconstruction.**

## 5 Conclusions and Future Work

In this work, we showed that Doppler shifts in entry vehicle radio communications can be used to estimate the position and velocity of the entry vehicle within the structure of an Extended or Unscented Kalman Filter. This process can be applied for reconstruction of planetary entry vehicles. We showed that certain modes of the velocity, such as east-west velocity in the Huygens case, will be more observable than others due to orbital alignment of Earth and other planetary bodies. Finally, we developed and implemented a Doppler tracking measurement model in the NewSTEP trajectory estimation software for use in future entry vehicle trajectory reconstructions. Some future applications of this tool could be the forthcoming Titan Dragonfly trajectory reconstruction in 2034 and other proposed missions to Venus where the spacecraft instrumentation might be limited.

An untapped data source from the Huygens dataset includes the Huygens Descent Imager described in [27]. A potential avenue for future work is to incorporate measurements from the downward-facing camera on the Huygens Descent Imager used by the DTWG to further improve the accuracy of the Huygens trajectory reconstruction results. Reconstruction of EDL flight using NewSTEP has shown descent imagery improving reconstruction (see [17]) and this Huygens dataset can improve the fidelity of the trajectory reconstruction.

## References


1. Misra, P. and Enge, P., *Global Positioning System: Signals, Measurements, and Performance (Revised Second Edition)*, Ganga-Jamuna Press, 2010.

2. Gebre-Egziabher, D. and Gleason, S., *GNSS Applications and Methods*, Artech House, 2009.

3. Kinman, P., "Doppler Tracking of Planetary Spacecraft," *IEEE Transactions on Microwave Theory and Techniques*, Vol. 40, No. 6, 2002, pp. 1199—1204. doi: 10.1109/22.141352

4. Farhani, S., *ZigBee Wireless Networks and Transceivers*, Chapter 5, Elsevier, Inc., 2008. doi: 10.1016/B978-0-7506-8393-7.X0001-5

5. Karlgaard, C. D., Beck, R. E., Derry, S. D., Brandon, J. M., Starr, B. R., Tartabini, P. V., and Olds, A. D., "Ares I-X Trajectory Reconstruction: Methodology and Results," *Journal of Spacecraft and Rockets*, Vol. 50, No. 3, 2013, pp. 641–661. doi: 10.2514/1.A32345

6. Karlgaard, C. D., Kutty, P., Schoenenberger, M., Munk, M. M., Little, A., Kuhl, C. A., and Shidner, J., "Mars Science Laboratory Entry Atmospheric Data System Trajectory and Atmosphere Reconstruction," *Journal of Spacecraft and Rockets*, Vol. 51, No. 4, 2014, pp. 1029–1047. doi: 10.2514/1.A32770

7. Karlgaard, C. D., Schoenenberger, M., Dutta, S., and Way, D. W., "Mars Entry, Descent, and Landing Instrumentation 2 Trajectory, Aerodynamics, and Atmo-

sphere Reconstruction," *Journal of Spacecraft and Rockets*, Vol. 60, No. 1, 2023, pp. 199—214. doi: 10.2514/1.A35440

8. Vedvik, S. and Karlgaard, C. D., "Iterated Sigma-Point Kalman Filtering for Trajectory Reconstruction," NASA TM-20240001235, March 2024.

9. Kremkau, F. W., "Doppler Principles," in *ASE's Comprehensive Echocardiography*, Elsevier Health Sciences, 2015, pp. 11.

10. Acton, C., "Ancillary Data Services of NASA's Navigation and Ancillary Information Facility," *Planetary and Space Science*, Vol. 44, No. 1, 1996, pp. 65—70. doi: 10.1016/0032-0633(95)00107-7

11. Acton, C., Bachman, N., Semenov, B., and Wright, E., "SPICE Tools Supporting Planetary Remote Sensing," *The International Archives of the Photogrammetry, Remote Sensing and Spatial Information Sciences*, Vol. 41, 2016, pp. 357—359. doi: 10.5194/isprs-archives-XLI-B4-357-2016

12. Acton, C., Bachman, N., Semenov, B., and Wright, E., "A Look Toward the Future in the Handling of Space Science Mission Geometry," *Planetary and Space Science*, Vol. 150, 2018, pp. 9–12. doi: 10.1016/j.pss.2017.02.013

13. Litvinov, D., Rudenko, V., Alakoz, A., Bach, U., Bartel, N., Belonenko, A., Belousov, K., Bietenholz, M., Biriukov, A., Carman, R., et al., "Probing the Gravitational Redshift with an Earth-Orbiting Satellite," *Physics Letters A*, Vol. 382, No. 33, 2018, pp. 2192–2198. doi: 10.1016/j.physleta.2017.09.014

14. Moriconi, M., "Special Theory of Relativity Through the Doppler Effect," *European Journal of Physics*, Vol. 27, No. 6, 2006, p. 1409. doi: 10.1088/0143-0807/27/6/015

15. Bird, M., "Atmospheric Attenuation of the Huygens S-Band Radio Signal During the Titan Descent," *Huygens: Science, Payload and Mission*, Edited by A. Wilson, ESA SP-1177, 1997, pp. 321–335.

16. Pensado, A., Robb, C., Winski, R., Williams, J., Belair, M., and Lorenz, R., "Assessing Huygens Probe Entry, Descent, and Landing at Titan Simulation Using Dragonfly Atmosphere Model," AIAA Paper 2025-2238, January 2025. doi: 10.2514/6.2025-2238

17. Deshmukh, R., Dutta, S., Korzun, A., DiNonno, J., Cheatwood, F. M., Karlgaard, C., and Fine, A., "Low-Earth Orbit Flight Test of an Inflatable Decelerator Modeling and Reconstruction," *Journal of Spacecraft and Rockets*, Vol. 62, No. 4, 2025, pp. 1387–1406. doi: 10.2514/1.A36197

18. Williams, R., Lugo, R., Marsh, S., Hoffman, J., Shidner, J., and Aguirre, J., "Enabling Thread Safety and Parallelism in the Program to Optimize Simulated Trajectories II," AIAA Paper 2023-0148, January 2023. doi: 10.2514/6.2023-0148

19. Bird, M., Allison, M., Asmar, S., Atkinson, D., Avruch, I., Dutta-Roy, R., Dzierma, Y., Edenhofer, P., Folkner, W., Gurvits, L., et al., "The Vertical Profile of Winds on Titan," *Nature*, Vol. 438, No. 7069, 2005, pp. 800–802. doi: 10.1038/nature04060

20. Dutta-Roy, R., "The Huygens Doppler Wind Experiment: A Titan Zonal Wind Retrieval Algorithm," Ph.D. Thesis, University of Bonn, August 2002.

21. Lorenz, R. D., Lebreton, J.-P., Leroy, A., and Pérez-Ayúcar, M., "Evolution of the Huygens Probe Spin During Parachute Descent," *Journal of Spacecraft and Rockets*, Vol. 58, No. 3, 2021, pp. 609–618. doi: 10.2514/1.A34818

22. Hathi, B., Ball, A. J., Colombatti, G., Ferri, F., Leese, M. R., Towner, M. C., Withers, P., Fulchigioni, M., and Zarnecki, J. C., "Huygens HASI Servo Accelerometer: A Review and Lessons Learned," *Planetary and Space Science*, Vol. 57, No. 12, 2009, pp. 1321–1333. doi: 10.1016/j.pss.2009.06.023

23. Clausen, K., Hassan, H., Verdant, M., Couzin, P., Huttin, G., Brisson, M., Sollazzo, C., and Lebreton, J.-P., "The Huygens Probe System Design," *Space Science Reviews*, Vol. 104, No. 1, 2002, pp. 155–189. doi: 10.1023/A:1023648925732

24. Atkinson, D. H., Kazeminejad, B., Lebreton, J.-P., Witasse, O., Pérez-Ayúcar, M., and Matson, D. L., "The Huygens Probe Descent Trajectory Working Group: Organizational Framework, Goals, and Implementation," *Planetary and Space Science*, Vol. 55, No. 13, 2007, pp. 1877–1885. doi: 10.1016/j.pss.2007.04.004

25. Lebreton, J.-P., and Matson, D., "The Huygens Probe: Science, Payload and Mission Overview," *Space Science Reviews*, Vol. 104, 2002, pp. 59–100. doi: 10.1023/A:1023657127549

26. Folkner, W., Asmar, S., Border, J., Franklin, G., Finley, S., Gorelik, J., Johnston, D., Kerzhanovich, V., Lowe, S., Preston, R., et al., "Winds on Titan from Ground-Based Tracking of the Huygens Probe," *Journal of Geophysical Research: Planets*, Vol. 111, No. E7, 2006. doi: 10.1029/2005JE002649

27. Karkoschka, E., Tomasko, M. G., Doose, L. R., See, C., McFarlane, E. A., Schröder, S. E., and Rizk, B., "DISR Imaging and the Geometry of the Descent of the Huygens Probe within Titan's Atmosphere," *Planetary and Space Science*, Vol. 55, No. 13, 2007, pp. 1896–1935. doi: 10.1016/j.pss.2007.04.019